

A Three-Scale Finite Element Investigation into the Effects of Tissue Mineralisation and Lamellar Organisation in Human Cortical and Trabecular Bone

T.J. Vaughan¹, C.T. McCarthy², L.M. McNamara^{1*}

¹ National Centre for Biomedical Engineering Sciences (NCBES) and the Department of Mechanical and Biomedical Engineering, National University of Ireland, Galway.

² Materials and Surface Science Institute (MSSI) and the Department of Mechanical and Aeronautical Engineering, University of Limerick, Limerick, Ireland.

Address for correspondence:

Dr. Laoise M. McNamara
Department of Mechanical and Biomedical Engineering
National University of Ireland Galway
Galway,
Ireland
Phone: (353) 91-492251
Fax: (353) 91-563991
Email: Laoise.McNamara@nuigalway.ie

Keywords of the paper: finite element homogenisation, composite materials, bone, composition, tissue structure

Abstract

Bone is an exceptional material that is lightweight for efficient movement but also exhibits excellent strength and stiffness imparted by a composite material of organic proteins and mineral crystals that are intricately organised on many scales. Experimental and computational studies have sought to understand the role of bone composition and organisation in regulating the biomechanical behaviour of bone. However, due to the complex hierarchical arrangement of the constituent materials, the reported experimental values for the elastic modulus of trabecular and cortical tissue have conflicted greatly. Furthermore finite element studies of bone have largely made the simplifying assumption that material behaviour was homogeneous or that tissue variability only occurred at the microscale based on grey values from micro-CT scans. Thus, it remains that the precise role of nanoscale tissue constituents and microscale tissue organisation is not fully understood and more importantly that these have never been incorporated together to predict bone fracture or implant outcome in a multiscale finite element framework. In this paper, a three-scale finite element homogenisation scheme is presented which enables the prediction of homogenised effective properties of tissue level bone from its fundamental nanoscale constituents of hydroxyapatite mineral crystals and organic collagen proteins. Two independent homogenisation steps are performed on representative volume elements which describe the local morphological arrangement of both the nanostructural and microstructural levels. This three-scale homogenisation scheme predicts differences in the tissue level properties of bone as a function of mineral volume fraction, mineral aspect ratio and lamellar orientation. These parameters were chosen to lie within normal tissue ranges derived from experimental studies, and it was found that the predicted stiffness properties at the lamellar level correlate well with experimental nanoindentation results from cortical and trabecular bone. Furthermore these studies show variations in mineral volume fraction, mineral crystal size and lamellar orientation could be responsible for previous discrepancies in experimental reports of tissue moduli. We propose that this novel multiscale modelling

approach can provide a more accurate description of bone tissue properties in continuum/organ level finite element models by incorporating information regarding tissue structure and composition from advanced imaging techniques. This approach could thereby provide a preclinical tool to predict bone mechanics following prosthetic implantation or bone fracture during disease.

1.0 Introduction

Bone is a naturally occurring composite material whose internal architecture represents a complex structural organisation of its constituent materials, which consist mainly of hydroxyapatite mineral crystals and organic collagen proteins. These constituent phases are hierarchically organised to provide a highly optimised structure which exhibits high stiffness and excellent resistance to fracture, while also being lightweight for efficient movement. Bone is assembled at various structural length scales from the nanoscale constituent level right up to the macroscale organ level (Figure 1). At the nanostructural level (<100 nm), bone may be considered to be a platelet-reinforced composite material, consisting of hydroxyapatite mineral crystals (reinforcement phase) distributed within organic collagen fibrils and noncollagenous proteins (compliant matrix phase), as shown in Figure 1 (a). At a sub-microstructural level (1-10 μm), bone is composed of many mineralised collagen fibrils which are unidirectionally aligned into packets known as lamellae, as shown in Figure 1 (b), much like a traditional fibre-reinforced composite ply. Bone is typically classified as either cortical or trabecular bone, based on the microstructural organisation of these lamellae. In cortical bone, lamellae are concentrically arranged around a central vascular channel (Haversian canal) and each successive lamella has alternating fibre orientations, thereby forming osteons, as shown in Figure 1 (c). In trabecular bone however, lamellae are organized almost parallel to their longitudinal direction and do not contain a central vascular channel, as shown in Figure 1 (d). Finally, at a macrostructural level, the combination of a cortical shell surrounding an internal trabecular bone network forms the organ level bone structure (i.e. whole bone), as shown in Figure 1 (e).

Bone is both an inhomogeneous and anisotropic material due the tissue composition, the organisation of tissue lamellae, and internal micro-architectures, such as blood vessels and cell pores, which vary considerably across anatomical locations (Bromage *et al.* 2003; Nazarian *et al.* 2007). Mechanical testing of trabecular and cortical bone tissue has been carried out using

3/4-point bending (Choi *et al.* 1990), buckling (Runkle and Pugh 1975; Townsend *et al.* 1975), cantilever beam tests (Mente and Lewis 1989), micro-tensile testing (Ryan and Williams 1989; Rho *et al.* 1993; Samelin *et al.* 1996; McNamara *et al.* 2005; McNamara *et al.* 2006a), ultrasonic measurement (Rho *et al.* 1993) and nanoindentation (Rho *et al.* 1997; Rho *et al.* 1999; Zysset *et al.* 1999; Hoffler *et al.* 2000; Ferguson *et al.* 2003; Ozcivici *et al.* 2008). Reported values for the elastic modulus of trabecular and cortical tissue from these studies have conflicted, with values ranging from 0.75GPa to 30GPa (Runkle and Pugh 1975; Townsend *et al.* 1975; Mente and Lewis 1989; Ryan and Williams 1989; Choi *et al.* 1990; Rho *et al.* 1993; Samelin *et al.* 1996; Rho *et al.* 1997; Rho *et al.* 1998; Rho *et al.* 1999; Zysset *et al.* 1999; Hoffler *et al.* 2000; Ferguson *et al.* 2003; McNamara *et al.* 2006a; Ozcivici *et al.* 2008; McNamara 2011). There is much contention regarding whether cortical and trabecular bone are fundamentally the same tissue, and that it is their tissue organisation that distinguishes their mechanical behaviour, or whether the tissue composition and mechanical properties are different between the two bone types.

While the variety of different mechanical test methods used may have contributed to the large range of values reported, other factors such as tissue structure and composition are also known to affect mechanical behaviour (Ascenzi and Bonucci 1976; Currey 1984; Hofmann *et al.* 2006; Brennan *et al.* 2011b). Currey (1984) showed that the degree of mineralisation in cortical bone correlated with its stiffness and load-bearing strength, while Ascenzi and Bonucci (1976) found that the intricate arrangement of collagen provides tensile strength, elasticity and toughness (capacity to absorb energy). Also, Hofmann *et al.* (2006) showed that in secondary osteons, the alternating orientations between lamellae gave rise to different stiffness values, even though the degree of mineralisation was similar for all lamellae. Importantly, these studies (Ascenzi and Bonucci 1976; Currey 1984; Hofmann *et al.* 2006; Brennan *et al.* 2011b) show that observed stiffness values in bone are sensitive to both microstructural composition, i.e. mineral/collagen content (Ascenzi and Bonucci 1976; Currey 1984), and also microstructural

organisation, i.e. lamellar orientation (Hofmann *et al.* 2006). Furthermore, significant compositional (Dickenson *et al.* 1981; Li and Aspden 1997; Boyde *et al.* 1998; Gadeleta *et al.* 2000; Zioupos 2000; Brennan *et al.* 2011a) and structural (Augat and Schorlemmer 2006) changes are known to arise during diseases such as osteoporosis. However, due to the complex hierarchical arrangement of the constituent materials, precisely how small changes in mineral/collagen composition can affect the mechanical behaviour at the level of the whole bone is not clear.

Computational methods have been widely used to predict bone failure during disease and after prosthetic implantation, but for many years these methods assumed that the material behaviour was homogeneous (Ulrich *et al.* 1998; Homminga *et al.* 2002; Vilayphiou *et al.* 2010) or that tissue variability occurred at the microscale based on grey values from micro-CT scans (Jaecques *et al.* 2004). More recently, various analytical (Porter 2004; Ji and Gao 2006; Hamed *et al.* 2010; Martínez-Reina *et al.* 2011) and computational (Ghanbari and Naghdabadi 2009; De Micheli and Witzel 2011; Yuan *et al.* 2011) models have been proposed in order to fully predict macroscopic behaviour based on the nanostructural constituents. Analytical approaches have included an energy-sharing model by Porter (2004) and a tension-shear chain model by Ji and Gao (2006). Multilevel step-by-step homogenisation schemes have been proposed by both Hamed *et al.* (2010) and Martínez-Reina *et al.* (2011), who used classical continuum micromechanics homogenisation schemes (e.g. Mori-Tanaka) at each analysis level to predict the effective properties of bone. Also, a comprehensive numerical homogenisation model has been developed, which predicts the mechanical behaviour of cortical bone as a function of a multitude of compositional and architectural parameters (Racila and Crolet 2007; Predoi-Racila and Crolet 2008). These analytical and numerical models have established microstructure-property relationships for bone tissue, such as the effect of porosity (Racila and Crolet 2007; Predoi-Racila and Crolet 2008; Martínez-Reina *et al.* 2011), mineral content (Porter 2004; Racila and Crolet 2007; Predoi-Racila and Crolet 2008; Martínez-Reina *et al.* 2011) and

mineral aspect ratio (Ji and Gao 2006) on mechanical behaviour. While such analytical approaches provide a crucial insight into the contribution of composition and tissue organisation, these studies are limited by the simplifications necessary to solve analytical solutions, most notably that geometries must be idealised and the parameters within the system are reduced to create a closed-form expression. More recently, finite element homogenisation approaches have been used to analyse the hierarchical structural arrangement of bone.

Ghanbari and Naghdabadi (2009) consider a two-dimensional Representative Volume Element (RVE) which represents the nanostructure as a platelet-reinforced composite material. Using finite element homogenisation, they report similar mechanical properties of lamellar bone tissue to both experimental values reported by Currey (2002) and the analytical results presented by Porter (2004). Also, Yuan *et al.* (2011) considered two- and three-dimensional representations of mineralised collagen fibrils to provide an insight into the role of phases and morphology of the nanostructure on mechanical behaviour. At a microstructural level, multiscale finite element models which analyse structural effects are limited to a small number of investigations into the importance of lamellar arrangements, such as those by De Micheli and Witzel (2011) and Nackenhorst (2006) or sub-lamellar arrangements, such as that carried out on various fibrillar arrays by Reisinger *et al.* (2011), for dictating the mechanical behaviour of bone.

While previous step-by-step analytical approaches have been used to analyse bone on three or more different length scales (Hamed *et al.* 2010; Martínez-Reina *et al.* 2011), to date, multiscale finite element investigations have been limited to predicting mechanical behaviour between two independent length scales, i.e. they predict tissue properties based on mineral content or variation in tissue organisation, but cannot account for both simultaneously (Ghanbari and Naghdabadi 2009; De Micheli and Witzel 2011; Reisinger *et al.* 2011; Yuan *et al.* 2011). However, both tissue composition and hierarchical organisation must be taken into account to fully predict bone mechanical properties (Rho *et al.* 1998; McNamara 2011). There

is a distinct need for computational methods that simultaneously incorporate multiscale variability in both tissue composition and organisation to fully predict bone mechanics during disease or for implant design purposes. Hence, this paper outlines a three-scale finite element homogenisation scheme, which enables the prediction of homogenised effective properties of cortical and trabecular human bone from their fundamental nanoscale constituents of hydroxyapatite mineral crystals and organic collagen proteins and also their organisation at the microstructural level. In order to achieve this, two independent homogenisation steps are carried out, firstly at the nanostructural level and subsequently at the microstructural level. By performing these successive homogenisation steps, this integrated approach collectively investigates the effects of both compositional (e.g. volume fraction of mineral phase) and architectural factors (e.g. lamellar orientation and distribution of mineral crystals) on tissue level mechanical behaviour.

2.0 Multiscale Analysis of Bone

2.1 Model Formulation

In this study, two levels of structural hierarchy are incorporated to represent the nanoscale and microscale structural length scales.

(i) Nanostructural Level: One-step homogenisation

At the nanostructural level, we model bone as a platelet-reinforced composite material, consisting of hydroxyapatite mineral crystals which are periodically distributed within organic collagen fibrils, as shown in Figures 2 (a) and (b). From this periodic representation of the nanostructural morphology, a representative volume element may be identified, as shown in Figure 2 (c), from which global material properties may be determined through a periodic homogenisation approach. In this RVE, the dimensions of the mineral crystals are initially assumed to be $50 \times 25 \times 3$ nm following TEM observations by Rubin *et al.* (2003). The spacing between each mineral crystal in both the 1- and 3-directions (see Figure 2 (a)) is initially assumed as 5nm (Porter 2004; Ghanbari and Naghdabadi 2009), while the distance between

crystals in the 2-direction depends upon the mineral volume fraction (MVF). The model was discretised using approximately 7500 six-noded wedge elements (C3D6) using a *sweep* meshing algorithm. This produced periodic mesh characteristics on opposing faces of the RVE (needed for implementation of periodic boundary conditions). It was assumed that the nanoscale constituents were of sufficient dimension such that a continuum-based modelling approach may be employed for each constituent, whereby both mineral and collagen phases were taken to be homogeneous and isotropic. The mechanical properties of the constituent materials (Katz 1971) are summarised in Table 1.

(ii) Microstructural Level: Two-step homogenisation

Cortical Bone:

At the microstructural level, it is assumed that osteons are composed of eight concentrically arranged lamellae, as shown in Figure 2 (d). The osteon diameter of 200 μm was chosen based on Rho *et al.* (1998), while the size of the Haversian canal (80 μm) and individual lamellar thickness (7.5 μm) was based on a similar osteon model which was previously developed by De Micheli and Witzel (2011). This representation assumes that the osteon is periodic in the longitudinal direction and has a repeating unit of (20 μm) thickness. The mesh characteristics for this model were similar to those outlined for the nanostructural model. It was assumed that the mineral content was uniformly distributed over the osteon, meaning that each lamella has the same constitutive behaviour which is derived from the homogenised results from the preceding length scale (nanostructural level). This behaviour was highly anisotropic which meant that for each lamella, the principal lamellar orientation was defined with respect to its inclination from the longitudinal axis of the osteon, as shown in Figure 2 (d). Here, a cross-ply osteon is shown, where the principal lamellar orientation varies between $+45^\circ/-45^\circ$ for each successive lamella.

Trabecular Bone:

In the trabecular arrangement, it is assumed that the lamellae are organised parallel to their longitudinal direction but the model does not contain a central vascular channel, as shown in Figure 2(e). This meant the outer diameter measured 120 μ m. Again, the mesh characteristics are similar to those previously described and the constitutive behaviour is initially assumed to be similar to cortical bone, whereby the mineral content is uniformly distributed over the cross-section of the trabeculae. However, due to the continuous remodelling process, it has been reported that the mineral content in trabecular struts is non-uniformly distributed over their cross-section (Fratzl *et al.* 2004; Brennan *et al.* 2011a; Brennan *et al.* 2011b). Fratzl *et al.* (2004) showed that in some superficial regions of trabeculae, the degree of mineralisation was almost half that of the centre region, due to the presence of newly formed tissue on the outer surfaces. Hence, a non-uniform distribution of mineral is also analysed whereby the mineral volume fraction is assumed to decrease linearly from the centre lamella (MVF_{centre}) to the outer lamella (MVF_{outer}), where $MVF_{\text{outer}} = (0.65)MVF_{\text{centre}}$. For example, in the case that the centre lamella has an $MVF_{\text{centre}} = 40\%$, then the outer lamella has a $MVF_{\text{outer}} = 26\%$ (Fratzl *et al.* 2004).

2.2 Periodic Homogenisation Approach

Periodic boundary conditions are applied to the RVE models to ensure a macroscopically homogeneous stress/displacement field exists across the boundaries of each RVE (Vaughan and McCarthy 2011a; Vaughan and McCarthy 2011b). These consist of a series of kinematic boundary ties which ensure that in deformed configurations, there is both stress and displacement continuity on opposing RVE boundaries which maintains spatial periodicity, allowing the micro to macro transition. In three-dimensions, the periodic boundary conditions may be expressed as,

$$\begin{aligned}
 \mathbf{u}(0, x_2, x_3) - \mathbf{u}(l, x_2, x_3) &= \mathbf{u}_1 \\
 \mathbf{u}(x_1, 0, x_3) - \mathbf{u}(x_1, h, x_3) &= \mathbf{u}_2 \\
 \mathbf{u}(x_1, x_2, 0) - \mathbf{u}(x_1, x_2, t) &= \mathbf{u}_3
 \end{aligned} \tag{1}$$

where \mathbf{u}_1 , \mathbf{u}_2 and \mathbf{u}_3 are the displacement vectors which relate the displacements on opposite faces of the RVE shown in Figure 2 (c), while l , h and t correspond to the RVE dimensions in the 1-, 2- and 3-directions, respectively. These conditions are used to impose a range of deformation modes on RVE models to characterise material behaviour. For example, longitudinal tensile loading is applied to the RVE in Figure 2 (c) by applying a relative displacement in the 1-direction (δ_l) such that $\mathbf{u}_1 = (\delta_l, 0, 0)$. This induces a uniaxial strain state in the RVE from which macroscopic quantities may be found by determining volume averages of resulting microscopic state variables, in this case the local stress and strain fields. In order to evaluate the average stresses ($\bar{\sigma}_{ij}$) and strains ($\bar{\varepsilon}_{ij}$) over the RVE the following relations from Vaughan and McCarthy (2010) were used,

$$\bar{\sigma}_{ij} = \frac{1}{V_{RVE}} \sum_{k=1}^n (\sigma_{ijk} V_k) \quad (2)$$

$$\bar{\varepsilon}_{ij} = \frac{1}{V_{RVE}} \sum_{k=1}^n (\varepsilon_{ijk} V_k) \quad (3)$$

where V_{RVE} is the volume of the RVE, k is the element number, V_k is the volume of element k in the finite element mesh, n is the total number of elements and σ_{ij} and ε_{ij} are the ij stresses and strains, respectively, in the element k (for a uniaxial strain state applied to an RVE in the 1-direction, as described above, it is the local stresses and strains acting in this loading direction which are considered, i.e. σ_{11} and ε_{11}). The effective properties can then determined using the averaged stress and strain quantities (i.e. $\bar{\sigma}_{ij}$ and $\bar{\varepsilon}_{ij}$) and then determining the relevant stress-strain ratio for any given loading condition, i.e.,

$$\bar{E}_{ij} = \frac{\bar{\sigma}_{ij}}{\bar{\varepsilon}_{ij}} \quad (4)$$

In a similar fashion, shear loading may be induced by applying a relative displacement in the 1-direction (δ_s) such that $\mathbf{u}_2 = (\delta_s, 0, 0)$. Following a similar procedure to that described above, the shear moduli (e.g. G_{12} , G_{23} and G_{31}) may be determined. Further information

regarding the periodic homogenisation approach may be found in (Van der Sluis *et al.* 2000; Segurado *et al.* 2003; Vaughan 2011).

At a nanostructural level, six loading cases are considered which fully characterised the anisotropic mechanical properties of lamellar bone. These consist of axial tensile loading applied to the RVE model in the 1-, 2- and 3-directions (Figure 2(c)) to determine the axial moduli (e.g. E_{11} , E_{22} and E_{33}) and Poisson's ratios (e.g. ν_{12} , ν_{23} , ν_{31} , ν_{21} , ν_{32} , and ν_{13}). Also, a simple shear load is applied to the RVE in the 1-, 2- and 3-directions (Figure 2(c)) to determine the shear moduli (e.g. G_{12} , G_{23} and G_{31}). It should be noted that no assumption of material symmetry is made prior to the analysis as each of these 12 material constants are determined independently of one another. It may be shown however that the mineral-collagen structure exhibits orthotropic behaviour and of the 12 material constants, only 9 are independent of one another (see Table 2). At a microstructural level, only one loading case is considered which consists of axial tensile loading to determine the longitudinal modulus of the osteon and trabecular models, shown in Figure 2 (d) and (e), respectively. The longitudinal modulus is calculated using the same homogenisation procedure described above (Equations 2-4) and for the osteon model, the volume of the Haversian canal (which carries zero stress) is included in the calculation. Thus, at the microstructural level, the modulus being determined could be considered analogous to that determined by a micro-tensile test.

2.3 *Parametric Analysis*

To investigate the mechanical implications of variations in tissue mineralisation and lamellar organisation, a number of parameter variation studies were performed. Specifically, these included studies on mineral volume fraction and mineral aspect ratio at the nanostructural level, while a study lamellar orientation was performed at the microstructural level.

(i) *Nanostructural Level*

The predicted effective properties of lamellar bone are considered as a function of mineral volume fraction (MVF), as this parameter has been found to vary significantly across different

anatomical locations (Nazarian *et al.* 2007) and with the onset of clinical diseases such as osteoporosis (Brennan *et al.* 2011a). To investigate this parameter, the spacing between the mineral crystals in the 2-direction (see Figure 2 (c)) was varied to predict the effective properties for MVFs which ranged from 20% to 50%. The effect of mineral aspect ratio on the homogenised effective properties was also investigated as the reported dimensions of the mineral crystals obtained through transmission electron microscopy have varied significantly (Robinson 1952; Weiner and Price 1986; Moradian-Oldak *et al.* 1991; Rubin *et al.* 2003). In addition to the 50×25×3nm mineral crystal, this investigation considers both larger (75×25×3nm) and smaller mineral crystals (25×25×3nm) to determine their effect on mechanical behaviour.

Finally, the effect of spacing between each crystals in the 1-direction is examined. Initially, the inter-crystal spacing in the 1-direction was assumed to be 5nm (Ghanbari and Naghdabadi 2009). However, to examine the effect of the inter-crystal spacing on the mechanical behaviour of the mineral-collagen structure, two further distances of 11nm and 17nm are also considered. In the case of the 17nm inter-crystal spacing, the model fulfils the axial periodicity of collagen structures which is thought to be close to 67nm (Jäger and Fratzl 2000) (note that for all other parameter studies, an inter-crystal spacing of 5nm was assumed based the similar behaviour of the mineral-collagen structure at each inter-crystal spacing examined, see results section).

(ii) Microstructural Level

Cortical bone:

The predicted tissue level properties of cortical bone are considered as a function of lamellar orientation as numerous different lamellar arrangements have been observed experimentally within osteons using circularly polarized light (CPL) microscopy (Skedros *et al.* 1996; Bromage *et al.* 2003; Goldman *et al.* 2003). The lamellar organisation within osteons is thought to be dependent on local loading characteristics (Skedros *et al.* 1996; Bromage *et al.* 2003; Goldman *et al.* 2003). Typically, in regions where tensile forces are dominant, the

preferred orientation of collagen fibres is in the longitudinal direction of the osteon, while a transverse orientation of collagen fibres has been observed in lamellar regions where compressive forces are prevalent (Skedros *et al.* 1996; Bromage *et al.* 2003; Goldman *et al.* 2003). In this investigation, in addition to the Cross-ply lamellar organisation, three further lamellar organisations were analysed and these may be identified as Longitudinal, Transverse and Alternating arrangements. These arrangements were originally proposed by Ascenzi and Bonucci (Ascenzi and Bonucci 1967) and they have been observed subsequently in numerous investigations (Skedros *et al.* 1996; Bromage *et al.* 2003; Goldman *et al.* 2003). The individual lamellar orientations for each of these arrangements are summarised in Table 3. Furthermore, a study has also been carried out which examines the effect of the ratio between the overall osteon diameter and the Haversian canal diameter. Initially, the diameter of the Haversian system was assumed to be 80 μm and to examine the impact of this parameter on the mechanical behaviour of the osteon, two further diameters of 60 μm and 100 μm are also considered. In this study, the overall diameter of the osteon remains unchanged (200 μm) while the thickness of the eight individual lamellae are adjusted in order to accommodate the varying Haversian canal diameters.

Trabecular bone:

This analysis examined the same lamellar arrangements as in the osteon model. Although these distinct types of lamellar organisations have not yet been identified in trabecular bone, Rinnerthaler *et al.* (1999) found using small angle x-ray scattering analysis (SAXS) that mineral crystal orientations in trabeculae, although predominantly aligned along the longitudinal axis, exhibit varying orientations which range from the longitudinal to the transverse directions. These results (Rinnerthaler *et al.* 1999) would suggest that similar lamellar orientations could exist in trabecular bone as appear in cortical bone (Skedros *et al.* 1996; Bromage *et al.* 2003; Goldman *et al.* 2003) and thus warrant investigation.

3.0 Results

3.1 Nanostructural Homogenisation Model

A multiscale finite element homogenisation approach was used to determine effective properties for lamellar bone by assuming that the nanostructure is composed of hydroxyapatite mineral crystals periodically distributed in a collagen protein, as shown in Figure 2 (c). The predicted effective properties for lamellar bone were considered as a function of volume fraction of the hydroxyapatite mineral crystals. The effect of mineral volume fraction (MVF) on the resulting axial moduli (e.g. E_{11} , E_{22} and E_{33}) is shown in Figure 3 (a), where an increase in axial modulus is observed with an increase in MVF. The magnitude of the axial modulus in each material direction is clearly related to the dimensions of the mineral crystal in that particular direction. Also plotted in Figure 3 (a) are the experimental results reported by (Mulder *et al.* 2008) who used nanoindentation to analyse the tissue stiffness of trabecular bone as a function of the degree of mineralisation in specimens taken from the mandibular chondylars of newborn pigs. The predicted shear moduli values also show an increase with MVF, as shown in Figure 3 (b). Here, at each MVF, the predicted properties for both G_{12} and G_{23} are very similar and are both much lower than the prediction of G_{13} , as shear loading in these directions is dominated by the more compliant collagen phase. Meanwhile, the model's prediction of G_{13} shows a stiffer response as the shear loading occurs perpendicular to the length of the relatively stiff mineral crystal. Table 2 lists the effective properties determined for the mineral-collagen nanostructure at 40% MVF, which are used to describe the behaviour of lamellar bone at the microstructural level.

This study also examined the effect of mineral crystal size, by varying the aspect ratio to examine larger ($75 \times 25 \times 3 \text{nm}$) and smaller crystals ($25 \times 25 \times 3 \text{nm}$), in addition to the $50 \times 25 \times 3 \text{nm}$ mineral crystal. The resulting effective properties are again expressed in terms of the MVF, as shown in Figure 3(c). Here, it is apparent that a high aspect ratio leads to an increased longitudinal modulus, as seen by the $75 \times 25 \times 3 \text{nm}$ model, which is in agreement with the

analytical model presented by Ji and Gao (2006). By resolving local stress and strain field within each unit cell analysed, it may be seen that the reason for this increase in modulus is that the larger mineral crystals facilitate a more effective stress transfer through the length of the crystal, allowing them to bear a much higher load, as shown by the longitudinal stress distributions in Figure 4. Here, each model has the same MVF (40%) and it is only the dimensions of the crystals which have been varied. The longitudinal stress carried by the 75×25×3nm crystal is almost 2.5 times greater than that carried by the 25×25×3nm crystal, resulting in a much higher predicted stiffness at each MVF, as shown in Figure 3 (c). It was found that the aspect ratio of crystals had a negligible effect on the stiffness in both the 2- and 3-directions (not shown). Also plotted in Figure 3 (c) are the experimental results reported by Gupta *et al.* (2006) who used nanoindentation to analyse the stiffness of both lamellar bone and interstitial bone in a human femoral mid-shaft as a function of its MVF. The results of Gupta *et al.* (2006) are expressed in terms of the reduced modulus determined from nanoindentation tests. However, these still show an appropriate relation in terms of the trends observed in the model's prediction of stiffness for each of the crystal dimensions analysed.

Finally, the effect of inter-crystal spacing on mechanical behaviour was examined by considering a number of different arrangements of the 50×25×3nm crystals. The distances between crystals which were considered were 5nm, 11nm and 17nm and the resulting effective properties in the longitudinal direction (1-direction) are shown in Figure 3 (d). Our results predict that inter-crystal spacing has a minimal effect on the mechanical behaviour of mineral-collagen structure and may be attributed to the staggered arrangement of the mineral crystals. The staggered arrangement means that the stress transfer between crystals is not significant, i.e. in Region A in Figure 4 (b), under axial loading in the 1-direction as the majority of load is carried through the adjacent crystal (i.e. above Region A). Thus, due to the relatively low stress carried in the inter-crystal region, the distance between crystals has quite a small effect on the mechanical properties in this particular mineral arrangement.

3.2 *Microstructural Homogenisation Model*

At a microstructural level, a successive homogenisation step was carried out to predict effective properties of various lamellar arrangements used to represent both an osteon and trabecula, given by Figures 2 (d) and (e), respectively. This step of the analysis used the results derived from the three-dimensional nano-composite model to define the anisotropic mechanical properties of each lamella in the microstructure. Each model considered four different lamellar configurations (Nackenhorst and Lenz 2005; Nackenhorst 2006; De Micheli and Witzel 2011) (details given in Table 3). The resulting effective properties of each lamellar arrangement for both the osteon and trabecular models are shown in Figures 5 (a) and (b) as a function of MVF. For the osteon model, shown in Figure 5 (a), it is clear that the homogenised effective properties are a function of lamellar orientation. The highest stiffness is obtained for the longitudinal osteon model, where the lamellae are orientated at $+15^{\circ}/-15^{\circ}$, which represents the scenario where the longitudinal axis of the mineral platelets would be most closely aligned with the long axis of the osteon. Conversely, the lowest stiffness is found for the transverse osteon, where the lamellae are orientated at $+75^{\circ}/-75^{\circ}$, which means the properties of the osteon are more likely to be dominated by the more compliant collagen matrix phase. Meanwhile, the cross-ply and alternating osteons exhibit similar properties which appear to be intermediate to those of the longitudinal and transverse osteons, as shown in Figure 5 (a). Also shown in Figure 5 (a) are the experimental stiffness values for both longitudinal and transverse osteon arrangements reported by Ascenzi and Bonnucci (1967) who performed micro-tensile testing of wet, fully calcified osteon specimens from a young donor. It should be noted that these results were evaluated through testing hemidiameteral osteon sections which would have a different void/solid ratio than the osteon models presented here (the effect of the void/solid ratio on osteon stiffness is discussed later). These appear here as horizontal lines, as details regarding the mineral content was unavailable. It is interesting that the experimental values for both osteon types intersect the model's predictions at $\sim 30\text{-}35\%$ MVF, which is close to the reported

mineral content in of cortical bone (e.g. the range of MVF measured by Gupta *et al.* (2006), see Figure 3 (c)). Also shown in Figure 5 (a) are the elastic properties predicted by the analytical approach used by Hamed *et al.* (2010), which are similar to those predicted by a longitudinal osteon arrangement.

The predicted effective properties from the trabecular model which had a uniform mineral distribution show similar trends to those of the osteon model, as shown in Figure 5 (b). The obtained stiffness values for each lamellar arrangement are slightly higher than their corresponding osteon arrangement at each MVF analysed due to the absence of the Haversian system. However, the trabecular model with a non-uniform mineral distribution, i.e. where $MVF_{\text{outer}} = (0.65)MVF_{\text{centre}}$, had lower tissue level stiffness values than that of cortical bone for a longitudinal lamellar arrangement at each MVF examined, as shown in Figure 5 (c). As this trabecular model had a non-uniform distribution of mineral content, the MVF values plotted in Figure 5 (c) correspond to the MVF of the centre lamella (i.e. MVF_{centre}).

The effect of mineral aspect ratio on the predicted properties of both a longitudinal and cross-ply osteon is shown in Figure 5 (d). The mineral aspect ratio has a pronounced effect on the predicted properties of the longitudinal osteon, similar to its effect on lamellar bone from the preceding length scale (see Figure 3 (c)), where, again, the 75x25x3nm crystal arrangement exhibits the highest stiffness. Its effect on the cross-ply osteon is less pronounced due to the off-axis alignment of the mineral crystals in this type of lamellar arrangement. It was found that the mineral aspect ratio had a similar effect on the predicted properties of the trabecular model for each lamellar arrangement discussed here (not shown). Meanwhile, it was found that the mineral aspect ratio had a negligible effect on the transverse arrangement in both the osteon and trabecular models (not shown), which is again due to the off-axis alignment of the mineral crystals.

Finally, the effect of the ratio between the Haversian canal diameter and the overall osteon diameter for a longitudinal osteon is shown in Figure 5 (e). The results of this study highlight

that a larger Haversian system reduces the overall osteon stiffness, as in the case of the 100 μm diameter canal shown in Figure 5 (e). The opposite is true in the case of the 60 μm diameter, where the osteon stiffness is larger due to increased volume of lamellar tissue in this arrangement. For all other osteon arrangements, a similar effect on the osteon stiffness was observed when the Haversian canal diameter was varied (not shown).

4.0 Discussion

In this paper, a three-scale homogenisation scheme has been outlined which estimates the effective properties of trabecular and cortical bone, based on finite element models defined at the nanostructural and microstructural level. The multiscale framework accounts for the combined contribution of both compositional (e.g. volume fraction of mineral phase) and structural (e.g. lamellar orientation and aspect ratio of mineral crystals) factors affecting the behaviour of bone tissue. Furthermore, by resolving local stress/strain fields at each material length scale, the model provides an insight into the mechanisms which contribute to the tissue level behaviour of bone. Collectively, the results predicted by this multiscale homogenisation model are a function of MVF, lamellar orientation and mineral aspect ratio and they exhibit a stiffness range which varies between 1.94-28.18 GPa. Interestingly, we see that the stiffness values predicted are within the range reported for both cortical and trabecular bone determined through various experimental testing methods. These results suggest that discrepancies between the experimentally derived tissue properties can easily be explained by variations in mineral volume fraction, mineral crystal size and lamellar orientation as the values for each of these investigated parameters were chosen to be within normal tissue ranges.

Several assumptions have been made at each length scale, which have facilitated the prediction of tissue level mechanical properties. At a nanostructural level, it was assumed that the morphology is comprised of periodically distributed hydroxyapatite mineral crystals embedded in an organic collagen phase. This represents a simplification of the actual nanostructural arrangement which has been reported to also contain water (Weiner and Wagner

1998) and non-collagenous proteins (NCPs) (Olszta *et al.* 2007). While some analytical approaches have considered these phases in their models (Hamed *et al.* 2010; Martínez-Reina *et al.* 2011), other finite element investigations (Ghanbari and Naghdabadi 2009; Yuan *et al.* 2011) assume a mineral-collagen morphology, similar to that presented here. Therefore it seems reasonable to assume that the effects of these nanoscale constituents, i.e. water and NCPs, have already been homogenised in the mechanical properties used to describe the behaviour of organic collagen phase and would not impact greatly on the results obtained.

At a microstructural level, the model makes a simplifying assumption that lamellar bone is composed of clearly aligned, parallel fibril layers, whose orientation alternates for each successive lamella. There are however recent observations which suggest that lamellar bone is composed of a series of sub-lamellar fibrillar layers, which exhibit various motifs, such as an orthogonal plywood pattern (Giraud-Guille 1988) (a 90° orientation between sub-lamellar fibrillar layers) or a twisted-plywood pattern (Giraud-Guille 1988) (a continuous rotation between sub-lamellar fibrillar layers). Using nano-indentation testing, Gupta *et al.* (2006) observed a rotational sub-lamellar fibril arrangement, which was mechanically characterised by a periodic modulation of the indentation modulus in the intra-lamellar region. Furthermore, Ziv *et al.* (1996) suggest a more complex intra-lamellar structural arrangement whereby varying crystal orientations might exist within the rotating collagen fibril network of the intra-lamellar region and would thus alter the transverse behaviour of the lamellar region. Reisinger *et al.* (2011) carried out a finite element study on the effect of different rotating collagen fibril arrangements on lamellar behaviour and concluded that a large variety of intra-lamellar patterns must exist. Due to ambiguity surrounding lamellar patterns, the model here assumes more classical behaviour where sub-lamellar fibrillar layers are aligned parallel to one another. Our multiscale framework could be used in future to examine further sub-lamellar and mineral crystal arrangements, but such analyses were beyond the scope of the current study.

The models describing the osteon and trabecular arrangements represent simplifications of typical *in vivo* geometries. In trabecular bone, the arrangement of lamellae is not ideally concentric due to the continuous remodelling process which results in scallop shaped lamellar packets forming on the outer surfaces of trabeculae. Furthermore, the diameter of individual trabeculae varies throughout their cross section and their profile is non-uniform due to the presence of resorption cavities, which have been shown to lead to significant local stress concentrations (McNamara *et al.* 2006b). Also, both osteons and trabeculae exhibit a certain level of porosity due to the presence of lacunar and canalicular cavities which have not been included in the current models. However, Mullins *et al.* (2007) showed that while lacunar cavities (accounting for 3% porosity) could cause a local strain amplification of up to seven times the applied global strain, their effect on the homogenised mechanical properties was less than 5%. As the focus of this analysis was to determine homogenised stiffness values for the tissue level, these simplifications were deemed acceptable in order to efficiently apply a periodic homogenisation approach to the microstructural models.

The key findings of this paper have related the effects of both microstructural and nanostructural morphology to the mechanical properties of bone tissue through a novel three-scale finite element homogenisation approach. The model's predictions of the mechanical properties at the lamellar level correlate well with experimental nanoindentation results from cortical (Gupta *et al.* 2006) and trabecular (Mulder *et al.* 2008) bone. The predictions of our model regarding mechanical behaviour at the tissue level are more difficult to validate as few experimental studies on individual osteons or trabeculae have characterised tissue properties as a function of either tissue mineralisation and/or collagen fibril orientation, with the exception of Ascenzi and Bonucci (1967). For their investigation, the stiffness of hemidiameteral osteon sections measuring approximately 50µm thick was evaluated as a function collagen fibril orientation. While Ascenzi and Bonucci's (1967) experimental conditions are not the same as the models presented here, as their specimens did not contain a Haversian canal, their study did

show that a longitudinal osteon exhibited a higher stiffness than an osteon with a transverse arrangement, which is also predicted by our model, as shown in Figure 5 (a). The predictions of the model developed in the current study also show similar trends to the previous numerical model of Predoi-Racila and Crolet (2008), whereby our model predicts a similar longitudinal stiffness for each osteon type analysed. Furthermore the dependence of the homogenised stiffness values with the volume percentage of the hydroxyapatite phase is in keeping with Predoi-Racila and Crolet (2008). A distinct advantage of this current study over previous analytical (Porter 2004; Ji and Gao 2006; Hamed *et al.* 2010; Martínez-Reina *et al.* 2011) and numerical (Predoi-Racila and Crolet 2008) models is that we have developed a framework that can be incorporated with the finite element method to predict tissue and whole bone behaviour by solving boundary value problems of microscale unit cells using a fully coupled periodic homogenisation approach. As each constituent is represented discretely, the approach allows local stress/strain fields within each of the unit cells to be resolved, facilitating a better understanding of certain microstructure-property relationships (e.g. details regarding stress transfer between constituents in various mineral-collagen arrangements and its effect of macroscopic behaviour), see Figures 3(c) and 4. We propose that the approach developed in this study could be applied to further understand the large discrepancies in reports of mechanical behaviour of bone tissue between different experimental test methods (Runkle and Pugh 1975; Townsend *et al.* 1975; Mente and Lewis 1989; Ryan and Williams 1989; Choi *et al.* 1990; Rho *et al.* 1993; Samelin *et al.* 1996; Rho *et al.* 1997; Rho *et al.* 1998; Rho *et al.* 1999; Zysset *et al.* 1999; Hoffler *et al.* 2000; Ferguson *et al.* 2003; McNamara *et al.* 2006a; Ozcivici *et al.* 2008; McNamara 2011), but also to decipher the impact of changes in tissue composition or structure during disease. From the results presented here, it is clear that a major contributor to this large range of experimentally reported stiffness values is the MVF (Figures 3 and 5). The mineral content of bone is known to vary with age (Augat and Schorlemmer 2006), anatomical location (Nazarian *et al.* 2007) and the onset of osteoporosis (Brennan *et al.* 2011a) meaning

that tissue level mechanics must change accordingly. Moreover, the distribution of mineral in trabecular bone is non-uniform, with superficial regions generally being less mineralised due to the continuous remodelling of the outer surfaces of trabecular packets (Fratzl *et al.* 2004; Brennan *et al.* 2011a; Brennan *et al.* 2011b). The results presented in Figure 5 highlight that it is this non-uniform distribution of mineral which contributes to the lower stiffness of trabecular bone compared to that of cortical bone. In fact, the model which assumed a uniform distribution of mineral content predicted higher stiffness values in trabecular bone when compared to cortical bone, which is generally not observed experimentally (McNamara 2011). It is also interesting that a larger mineral aspect ratio (i.e. larger crystal size) resulted in higher stiffness values predicted at the tissue level (Figures 5 (c) and (d)), due to a more effective stress transfer through the length of the crystal (Figure 4). Given that experimental observations of mineral crystal lengths have varied from between 10nm to 150nm (Robinson 1952; Weiner and Price 1986; Moradian-Oldak *et al.* 1991; Rubin *et al.* 2003), the findings here highlight that this nanostructural parameter could be as much a contributor to the mechanical behaviour as the mineral content (although by their very nature, the two factors are inextricably linked). Furthermore, although there is disagreement as to whether osteoporosis affects the mineral crystal size (Rubin *et al.* 2003), transmission electron microscopy (TEM) studies (Baud *et al.* 1976; Boskey 1990) and Fourier transform infrared micro-spectroscopy (FTRIM) (Gadeleta *et al.* 2000) have reported that mineral crystal size increases with the onset of osteoporosis and the results here suggest that the crystal dimensions would contribute to changes in the tissue level response in osteoporotic bone.

These results have also shown that the tissue level properties are further affected by the lamellar arrangement within the microstructure, with longitudinal arrangements leading to higher predicted stiffness values than either alternating, cross-ply or transverse arrangements. Given that both longitudinal and transverse osteons are found in the mid-shafts of long bones (Bromage *et al.* 2003), the results here suggest that significant local stiffness variations would

exist across the mid-shaft, as seen in Figures 5 (a) and (b) where stiffness values for transverse arrangements are approximately half those of longitudinal arrangements. The results of our study also show that the diameter of the Haversian canal of the osteon, is an important factor in determining material behaviour, see Figure 5 (e), and in particular that the overall void to solid ratio of the osteon governs the mechanical behaviour of the osteon.

These results have highlighted the collective contribution of tissue mineralisation and lamellar arrangement on tissue level response. For example, if a micro-tensile test determined that the tissue level stiffness of trabecular bone was 10 GPa and that cortical bone was 20GPa, the results shown in Figure 5 demonstrate that there are a multitude of combinations of mineral content, mineral size and lamellar arrangements which could explain these values. Furthermore, these studies demonstrate that a wide range of bone tissue properties can indeed occur in both trabecular and cortical bone tissue, and explain the discrepancies from previous studies. It is therefore important to consider the each of these factors when evaluating tissue level mechanics of both cortical and trabecular bone. Advanced imaging techniques, such as transmission electron microscopy (TEM), circularly polarised light (CPL) microscopy and backscatter electron imaging (BEI), can now provide quantitative information on details such as fibre orientation patterns and mineral content within the tissue structure. The multiscale model developed herein could prove useful in accurately predicting mechanical properties based on results from these types of imaging characterisations at different anatomical locations.

Finite element methods have previously been employed to predict fracture risk in patient specific cases (Orwoll *et al.* 2009). Current finite element approaches use empirical methods (Morgan *et al.* 2003) to define isotropic mechanical behaviour based on observed bone mineral density values derived from the grey values in μ CT scans. The multiscale model developed herein has shown that tissue behaviour is highly anisotropic and dependant on factors other than bone mineral density. It could therefore prove useful in describing mechanical behaviour in continuum level finite element models by providing quantitative stiffness values for different

anatomical locations within the bone structure, based on the degree of mineralisation and structural organisation at that particular location and thus overcome the limitations of analytical methods. Such models could inform diagnosis and treatment of clinical diseases, such as osteoporosis.

5.0 Conclusions

In this study we develop a three-scale finite element homogenisation scheme to predict tissue level elastic properties of cortical and trabecular bone as a function of mineral volume fraction, mineral aspect ratio and lamellar orientation. These parameters were chosen to lie within normal tissue ranges derived from experimental studies, and it was found that the predicted stiffness properties at the lamellar level correlate well with experimental nanoindentation results from cortical (Gupta *et al.* 2006) and trabecular (Mulder *et al.* 2008) bone. These findings highlight the wide ranging effect of tissue mineralisation and lamellar orientation on tissue level behaviour and provide a suitable finite element framework that can account for the combined contribution of these parameters. These studies also shed light on previous discrepancies in experimental reports of tissue moduli and reveal that variations in mineral volume fraction, mineral crystal size and lamellar orientation could explain these differences. Given the dependence of tissue mineralisation and lamellar arrangement with age (Augat and Schorlemmer 2006), anatomical location (Nazarian *et al.* 2007) and clinical disease (Brennan *et al.* 2011a) it is clear that bone composition and organisation need to be considered before meaningful predictions of the tissue level response can be determined. With the aid of advanced imaging techniques, it is thought that this multiscale modelling approach could be used to provide a more accurate description of mechanical properties in continuum/organ level finite element models.

Acknowledgements

This authors wish to acknowledge the funding provided by the European Research Council (ERC) under grant number 258992 (BONEMECHBIO).

References

- Ascenzi, A. and E. Bonucci, 1967. The tensile properties of single osteons. *The Anatomical Record* 158(4), 375-386.
- Ascenzi, A. and E. Bonucci, 1976. Relationship between ultrastructure and "pin test" in osteons. *Clin Orthop Relat Res*(121), 275-294.
- Augat, P. and S. Schorlemmer, 2006. The role of cortical bone and its microstructure in bone strength. *Age and Ageing* 35(suppl 2), ii27-ii31.
- Baud, C. A., J. A. Pouezat and H. J. Tochon Danguy, 1976. Quantitative analysis of amorphous and crystalline bone tissue mineral in women with osteoporosis. *Calcified Tissue International* 21(Sup.), 452-456.
- Boskey, A. L., 1990. Bone mineral and matrix. Are they altered in osteoporosis? *Orthopedic Clinics of North America* 21(1), 19-29.
- Boyde, A., J. E. Compston, J. Reeve, K. L. Bell, B. S. Noble, S. J. Jones and N. Loveridge, 1998. Effect of estrogen suppression on the mineralization density of iliac crest biopsies in young women as assessed by backscattered electron imaging. *Bone* 22(3), 241-250.
- Brennan, M., J. Gleeson, M. Browne, F. O'Brien, P. Thurner and L. McNamara, 2011a. Site specific increase in heterogeneity of trabecular bone tissue mineral during oestrogen deficiency. *European Cells & Materials Journal* 21, 396-406.
- Brennan, O., O. D. Kennedy, T. C. Lee, S. M. Rackard, F. J. O'Brien and L. M. McNamara, 2011b. The effects of estrogen deficiency and bisphosphonate treatment on tissue mineralisation and stiffness in an ovine model of osteoporosis. *Journal of Biomechanics* 44(3), 386-390.
- Bromage, T. G., H. M. Goldman, S. C. McFarlin, J. Warshaw, A. Boyde and C. M. Riggs, 2003. Circularly polarized light standards for investigations of collagen fiber orientation in bone. *The Anatomical Record Part B: The New Anatomist* 274B(1), 157-168.
- Choi, K., J. Kuhn, M. Ciarelli and S. Goldstein, 1990. The elastic moduli of human subchondral, trabecular, and cortical bone tissue and the size-dependency of cortical bone modulus. *J Biomech* 23(11), 1103-1113.
- Currey, J. D., 1984. Effects of differences in mineralization on the mechanical properties of bone. *Philos Trans R Soc Lond B Biol Sci* 304(1121), 509-518.
- Currey, J. D. (2002). Bones: structure and mechanics. New Jersey, Princeton University Press.
- De Micheli, P. O. and U. Witzel, 2011. Microstructural mechanical study of a transverse osteon under compressive loading: The role of fiber reinforcement and explanation of some geometrical and mechanical microscopic properties. *Journal of Biomechanics* 44(8), 1588-1592.
- Dickenson, R. P., W. C. Hutton and J. R. Stott, 1981. The mechanical properties of bone in osteoporosis. *J Bone Joint Surg Br* 63-B(2), 233-238.
- Ferguson, V., A. Bushby and A. Boyde, 2003. Nanomechanical properties and mineral concentration in articular calcified cartilage and subchondral bone. *J Anat* 203(2), 191-202.
- Fratzl, P., H. S. Gupta, E. P. Paschalis and P. Roschger, 2004. Structure and mechanical quality of the collagen-mineral nano-composite in bone. *Journal of Materials Chemistry* 14(14), 2115-2123.
- Gadeleta, S. J., A. L. Boskey, E. Paschalis, C. Carlson, F. Menschik, T. Baldini, M. Peterson and C. M. Rimnac, 2000. A physical, chemical, and mechanical study of lumbar vertebrae from normal,

- ovariectomized, and nandrolone decanoate-treated cynomolgus monkeys (*macaca fascicularis*). *Bone* 27(4), 541-550.
- Ghanbari, J. and R. Naghdabadi, 2009. Nonlinear hierarchical multiscale modeling of cortical bone considering its nanoscale microstructure. *Journal of Biomechanics* 42(10), 1560-1565.
- Giraud-Guille, M., 1988. Twisted plywood architecture of collagen fibrils in human compact bone osteons. *Calcified Tissue International* 42(3), 167-180.
- Goldman, H. M., T. G. Bromage, C. D. L. Thomas and J. G. Clement, 2003. Preferred collagen fiber orientation in the human mid-shaft femur. *The Anatomical Record Part A: Discoveries in Molecular, Cellular, and Evolutionary Biology* 272A(1), 434-445.
- Gupta, H. S., U. Stachewicz, W. Wagermaier, P. Roschger, H. D. Wagner and P. Fratzl, 2006. Mechanical modulation at the lamellar level in osteonal bone. *Journal of Materials Research* 21, pp 1913-1921
- Hamed, E., Y. Lee and I. Jasiuk, 2010. Multiscale modeling of elastic properties of cortical bone. *Acta Mechanica* 213(1), 131-154.
- Hoffler, C., K. Moore, K. Kozloff, P. Zysset, M. Brown and S. Goldstein, 2000. Heterogeneity of bone lamellar-level elastic moduli. *Bone* 26(6), 603-609.
- Hofmann, T., F. Heyroth, H. Meinhard, W. Fränzel and K. Raum, 2006. Assessment of composition and anisotropic elastic properties of secondary osteon lamellae. *Journal of Biomechanics* 39(12), 2282-2294.
- Homminga, J., B. R. McCreadie, T. E. Ciarelli, H. Weinans, S. A. Goldstein and R. Huiskes, 2002. Cancellous bone mechanical properties from normals and patients with hip fractures differ on the structure level, not on the bone hard tissue level. *Bone* 30(5), 759-764.
- Jaecques, S. V. N., H. Van Oosterwyck, L. Muraru, T. Van Cleynenbreugel, E. De Smet, M. Wevers, I. Naert and J. Vander Sloten, 2004. Individualised, micro CT-based finite element modelling as a tool for biomechanical analysis related to tissue engineering of bone. *Biomaterials* 25(9), 1683-1696.
- Jäger, I. and P. Fratzl, 2000. Mineralized Collagen Fibrils: A Mechanical Model with a Staggered Arrangement of Mineral Particles. *Biophysical Journal* 79(4), 1737-1746.
- Ji, B. and H. Gao, 2006. Elastic properties of nanocomposite structure of bone. *Composites Science and Technology* 66(9), 1212-1218.
- Katz, J. L., 1971. Hard tissue as a composite material—I. Bounds on the elastic behavior. *Journal of Biomechanics* 4(5), 455-473.
- Li, B. and R. Aspden, 1997. Material properties of bone from the femoral neck and calcar femorale of patients with osteoporosis or osteoarthritis. *Osteoporos Int* 7(5), 450-456.
- Martínez-Reina, J., J. Domínguez and J. García-Aznar, 2011. Effect of porosity and mineral content on the elastic constants of cortical bone: a multiscale approach. *Biomechanics and Modeling in Mechanobiology* 10(3), 309-322.
- McNamara, L. (2011). Bone as a Material. *Comprehensive Biomaterials*. Paul Ducheyne, Kevin E. Healy, Dietmar E. Hutmacher, David E. Grainger and C. J. Kirkpatrick.
- McNamara, L. M., A. G. Ederveen, C. G. Lyons, C. Price, M. B. Schaffler, H. Weinans and P. J. Prendergast, 2006a. Strength of cancellous bone trabecular tissue from normal, ovariectomized and drug-treated rats over the course of ageing. *Bone* 39(2), 392-400.

- McNamara, L. M., P. J. Prendergast and M. B. Schaffler, 2005. Bone tissue material properties are altered during osteoporosis. *J Musculoskelet Neuronal Interact* 5(4), 342-343.
- McNamara, L. M., J. C. Van der Linden, H. Weinans and P. J. Prendergast, 2006b. Stress-concentrating effect of resorption lacunae in trabecular bone. *Journal of Biomechanics* 39(4), 734-741.
- Mente, P. and J. Lewis, 1989. Experimental method for the measurement of the elastic modulus of trabecular bone tissue. *J Orthop Res* 7(3), 456-461.
- Moradian-Oldak, J., S. Weiner, L. Addadi, W. J. Landis and W. Traub, 1991. Electron imaging and diffraction study of individual crystals of bone, mineralized tendon and synthetic carbonate apatite. *Connective Tissue Research* 25(3-4), 219-228.
- Morgan, E. F., H. H. Bayraktar and T. M. Keaveny, 2003. Trabecular bone modulus–density relationships depend on anatomic site. *Journal of Biomechanics* 36(7), 897-904.
- Mulder, L., J. H. Koolstra, J. M. J. den Toonder and T. M. G. J. van Eijden, 2008. Relationship between tissue stiffness and degree of mineralization of developing trabecular bone. *Journal of Biomedical Materials Research Part A* 84A(2), 508-515.
- Mullins, L. P., J. P. McGarry, M. S. Bruzzi and P. E. McHugh, 2007. Micromechanical modelling of cortical bone. *Computer Methods in Biomechanics and Biomedical Engineering* 10(3), 159-169.
- Nackenhorst, U., 2006. *Computational Methods for Studies on the Biomechanics of Bones Foundations of Civil and Environmental Engineering* 7.
- Nackenhorst, U. and C. Lenz, 2005. Biomechanics of bones on various length scales. *PAMM* 5(1), 31-34.
- Nazarian, A., J. Muller, D. Zurakowski, R. Müller and B. D. Snyder, 2007. Densitometric, morphometric and mechanical distributions in the human proximal femur. *Journal of Biomechanics* 40(11), 2573-2579.
- Olszta, M. J., X. Cheng, S. S. Jee, R. Kumar, Y.-Y. Kim, M. J. Kaufman, E. P. Douglas and L. B. Gower, 2007. Bone structure and formation: A new perspective. *Materials Science and Engineering: R: Reports* 58(3-5), 77-116.
- Orwoll, E. S., L. M. Marshall, C. M. Nielson, S. R. Cummings, J. Lapidus, J. A. Cauley, K. Ensrud, N. Lane, P. R. Hoffmann, D. L. Kopperdahl and T. M. Keaveny, 2009. Finite Element Analysis of the Proximal Femur and Hip Fracture Risk in Older Men. *Journal of Bone and Mineral Research* 24(3), 475-483.
- Ozcivici, E., S. Ferreri, Y. Qin and S. Judex, 2008. Determination of bone's mechanical matrix properties by nanoindentation. *Methods Mol Biol* 455, 323-334.
- Porter, D., 2004. Pragmatic multiscale modelling of bone as a natural hybrid nanocomposite. *Materials Science and Engineering A* 365(1-2), 38-45.
- Predoi-Racila, M. and J. M. Crolet, 2008. Human cortical bone: the SiNuPrOs model. *Computer Methods in Biomechanics and Biomedical Engineering* 11(2), 169-187.
- Racila, M. and J. M. Crolet, 2007. Nano and Macro Structure of Cortical Bone: Numerical Investigations. *Mechanics of Advanced Materials and Structures* 14(8), 655-663.
- Reisinger, A., D. Pahr and P. Zysset, 2011. Elastic anisotropy of bone lamellae as a function of fibril orientation pattern. *Biomechanics and Modeling in Mechanobiology* 10(1), 67-77.

- Rho, J.-Y., L. Kuhn-Spearing and P. Zioupos, 1998. Mechanical properties and the hierarchical structure of bone. *Medical Engineering & Physics* 20(2), 92-102.
- Rho, J., R. Ashman and C. Turner, 1993. Young's modulus of trabecular and cortical bone material: ultrasonic and microtensile measurements. *J Biomech* 26(2), 111-119.
- Rho, J., M. n. Roy, T. Tsui and G. Pharr, 1999. Elastic properties of microstructural components of human bone tissue as measured by nanoindentation. *J Biomed Mater Res* 45(1), 48-54.
- Rho, J., T. Tsui and G. Pharr, 1997. Elastic properties of human cortical and trabecular lamellar bone measured by nanoindentation. *Biomaterials* 18(20), 1325-1330.
- Rinnerthaler, S., P. Roschger, H. F. Jakob, A. Nader, K. Klaushofer and P. Fratzl, 1999. Scanning Small Angle X-ray Scattering Analysis of Human Bone Sections. *Calcified Tissue International* 64(5), 422-429.
- Robinson, R. A., 1952. An electron-microscopic study of the crystalline inorganic component of bone and its relationship to the organic matrix. *The Journal of bone and joint surgery. American* volume 34-A(2), 389-435; passim.
- Rubin, M. A., I. Jasiuk, J. Taylor, J. Rubin, T. Ganey and R. P. Apkarian, 2003. TEM analysis of the nanostructure of normal and osteoporotic human trabecular bone. *Bone* 33(3), 270-282.
- Runkle, J. and J. Pugh, 1975. The micro-mechanics of cancellous bone. II. Determination of the elastic modulus of individual trabeculae by a buckling analysis. *Bull Hosp Joint Dis* 36(1), 2-10.
- Ryan, S. and J. Williams, 1989. Tensile testing of rodlike trabeculae excised from bovine femoral bone. *J Biomech* 22(4), 351-355.
- Samelin, N., W. Köller, R. Ascherl and R. Gradinger, 1996. [A method for determining the biomechanical properties of trabecular and spongiosa bone tissue]. *Biomed Tech (Berl)* 41(7-8), 203-208.
- Segurado, J., C. Gonzalez and J. Llorca, 2003. A numerical investigation of the effect of particle clustering on the mechanical properties of composites. *Acta Materialia* 51(8), 2355-2369.
- Skedros, J. G., M. W. Mason, M. C. Nelson and R. D. Bloebaum, 1996. Evidence of structural and material adaptation to specific strain features in cortical bone. *The Anatomical Record* 246(1), 47-63.
- Townsend, P., R. Rose and E. Radin, 1975. Buckling studies of single human trabeculae. *J Biomech* 8(3-4), 199-201.
- Ulrich, D., B. van Rietbergen, H. Weinans and P. Rügsegger, 1998. Finite element analysis of trabecular bone structure: a comparison of image-based meshing techniques. *Journal of Biomechanics* 31(12), 1187-1192.
- Van der Sluis, O., P. J. G. Schreurs, W. A. M. Brekelmans and H. E. H. Meijer, 2000. Overall behaviour of heterogeneous elastoviscoplastic materials: effect of microstructural modelling. *Mechanics of Materials* 32(8), 449-462.
- Vaughan, T. (2011). *Micromechanical Modelling of Damage and Failure in Fibre Reinforced Composites under Loading in the Transverse Plane. Mechanical, Aeronautical & Biomedical Engineering Dept. Limerick, University of Limerick. **PhD Thesis.***
- Vaughan, T. J. and C. T. McCarthy, 2010. A combined experimental–numerical approach for generating statistically equivalent fibre distributions for high strength laminated composite materials. *Composites Science and Technology* 70(2), 291-297.

- Vaughan, T. J. and C. T. McCarthy, 2011a. Micromechanical modelling of the transverse damage behaviour in fibre reinforced composites. *Composites Science and Technology* 71(3), 388-396.
- Vaughan, T. J. and C. T. McCarthy, 2011b. A micromechanical study on the effect of intra-ply properties on transverse shear fracture in fibre reinforced composites. *Composites Part A: Applied Science and Manufacturing* 42(9), 1217-1228.
- Vilayphiou, N., S. Boutroy, E. Sornay-rendu, B. Van rietbergen, F. Munoz, P. D. Delmas and R. Chapurlat, 2010. Finite element analysis performed on radius and tibia HR-pQCT images and fragility fractures at all sites in postmenopausal women. *Bone* 46(4), 1030-1037.
- Weiner, S. and P. Price, 1986. Disaggregation of bone into crystals. *Calcified Tissue International* 39(6), 365-375.
- Weiner, S. and H. D. Wagner, 1998. The material bone: Structure mechanical function relations. *Annual Review of Materials Science* 28, 271-298.
- Yuan, F., S. Stock, D. Haeffner, J. Almer, D. Dunand and L. Brinson, 2011. A new model to simulate the elastic properties of mineralized collagen fibril. *Biomechanics and Modeling in Mechanobiology* 10(2), 147-160.
- Zioupos, P., Aspden, RM (2000). Density, material quality and quantity issues in OP cancellous bone. 12th Conference of the European Society of Biomechanics, Dublin, Ireland, Royal Academy of Medicine in Ireland.
- Ziv, V., H. D. Wagner and S. Weiner, 1996. Microstructure-microhardness relations in parallel-fibered and lamellar bone. *Bone* 18(5), 417-428.
- Zysset, P., X. Guo, C. Hoffler, K. Moore and S. Goldstein, 1999. Elastic modulus and hardness of cortical and trabecular bone lamellae measured by nanoindentation in the human femur. *J Biomech* 32(10), 1005-1012.

Figures

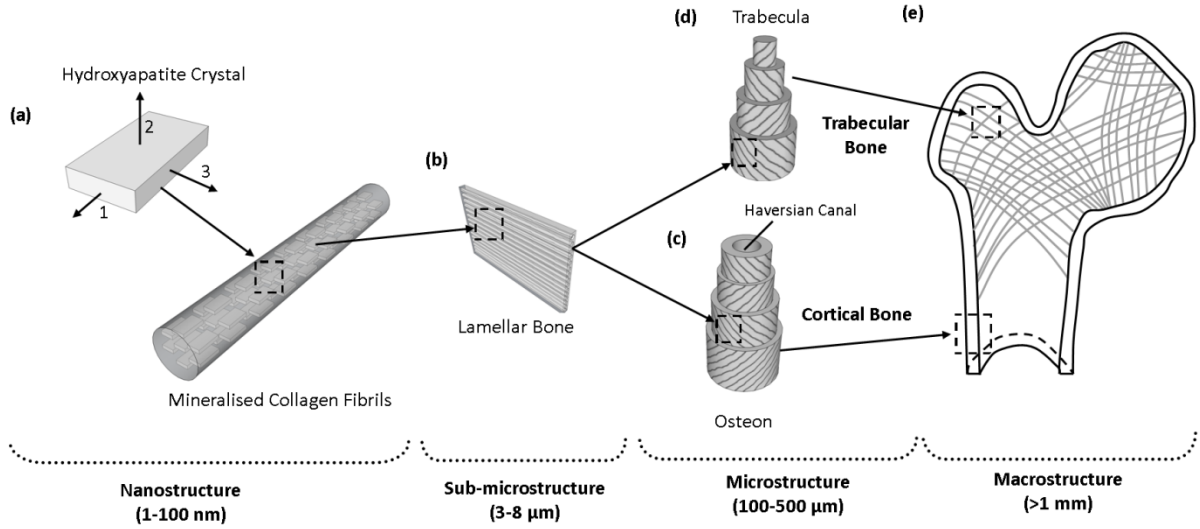


Figure 1: Hierarchical structure of bone

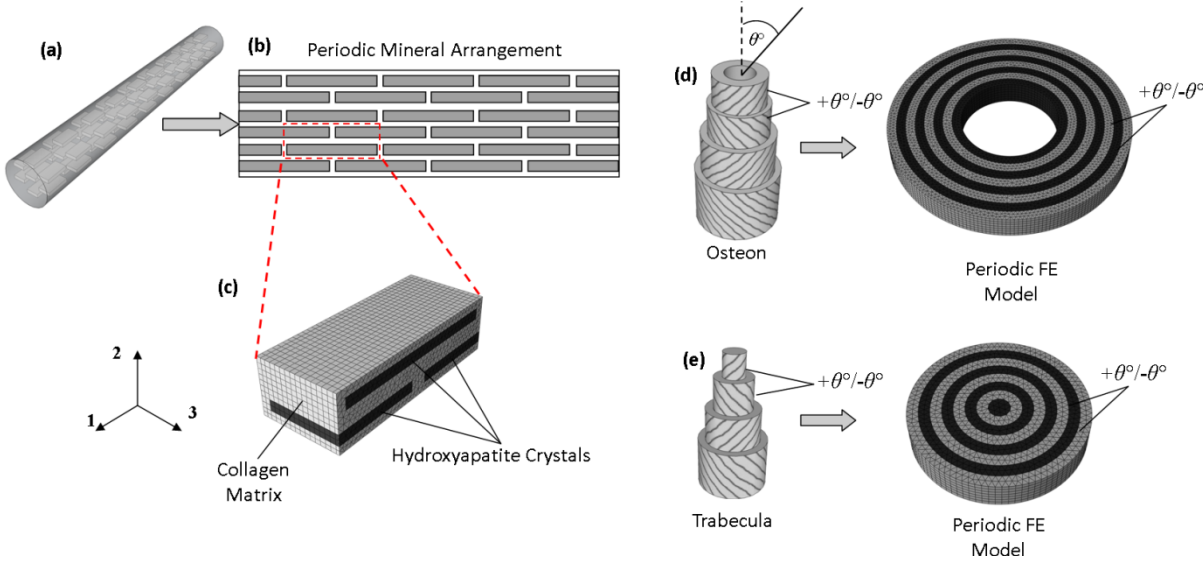


Figure 2: Multiscale homogenisation procedure used to predict the tissue level elastic properties (a) mineralised collagen fibril (b) periodic distribution of hydroxyapatite crystals in organic collagen matrix (c) representative volume element of nanoscale constituents (d) periodic osteon model and (e) periodic trabecular model.

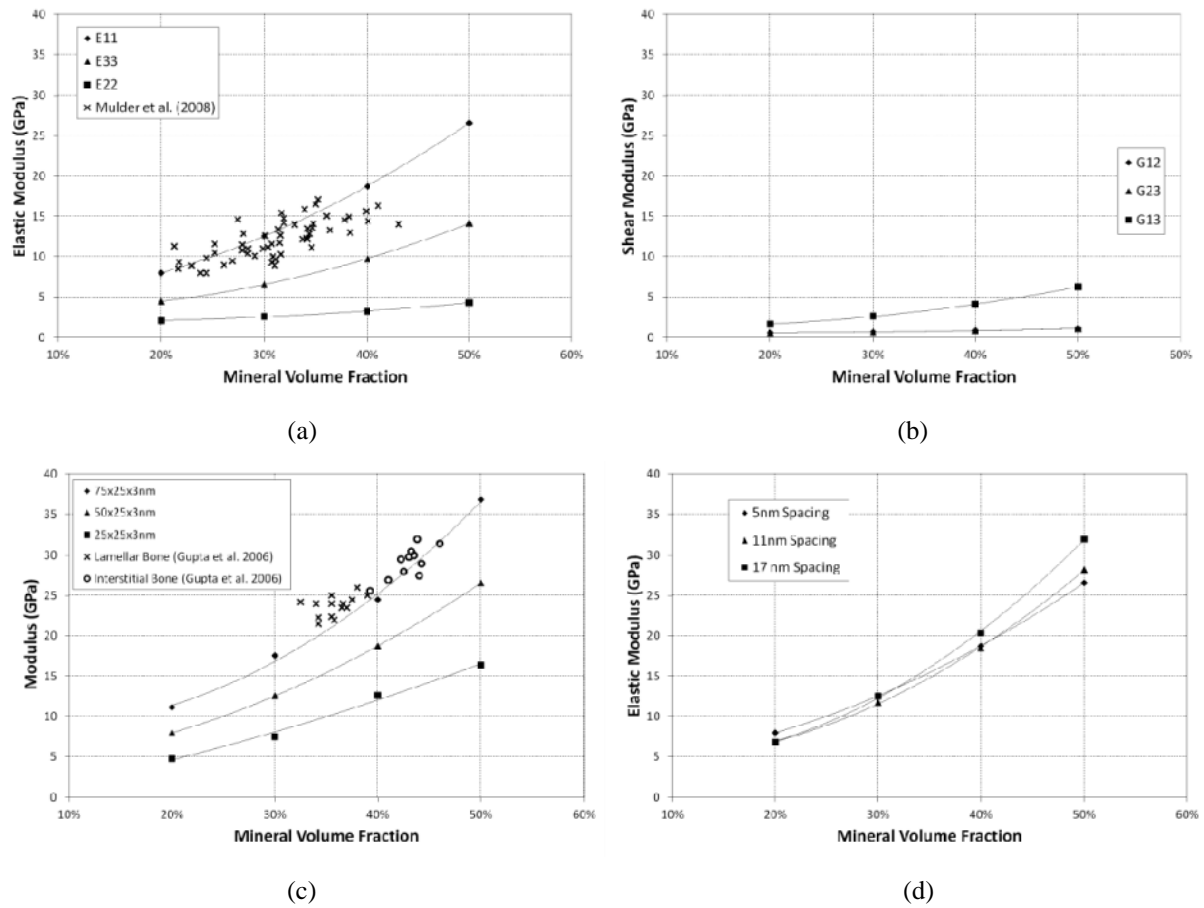


Figure 3: Results from one-step homogenisation which predicts the properties of lamellar bone as a function of mineral volume fraction: (a) Axial modulus in each of the material directions (b) shear modulus in each material direction (c) effect of the crystal aspect ratio on predicted elastic modulus in the 1-direction and (d) effect of the inter-crystal spacing on predicted elastic modulus in the 1-direction (a second-order polynomial trendline has been fit to each set of data points).

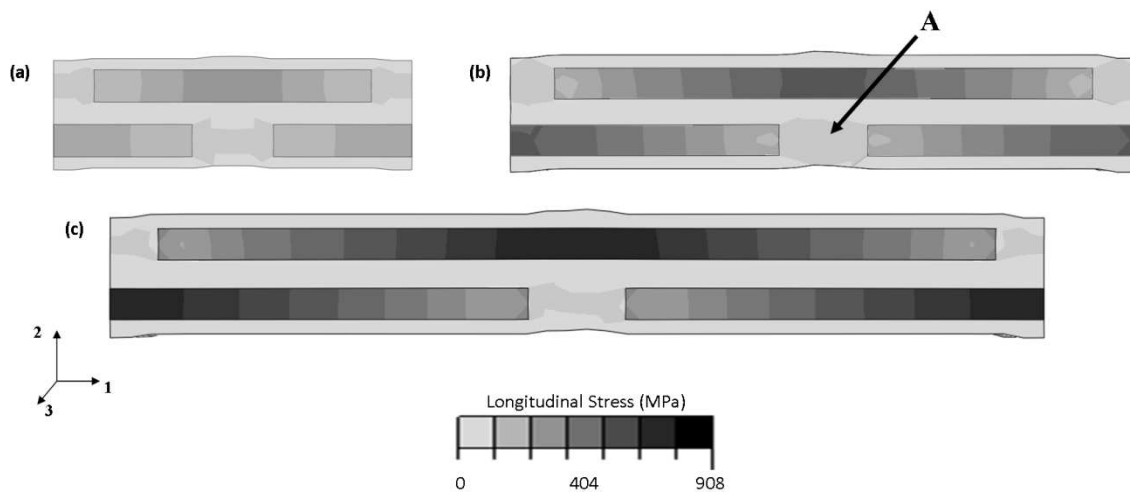


Figure 4: Longitudinal stress distribution in representative volume elements which had a mineral volume fraction of 40% for each of the crystal dimensions studied (a) $25 \times 25 \times 3$ nm (b) $50 \times 25 \times 3$ nm and (c) $75 \times 25 \times 3$ nm (Note: A macroscopic strain of 1% was applied in the 1-direction to each of these representative volume elements).

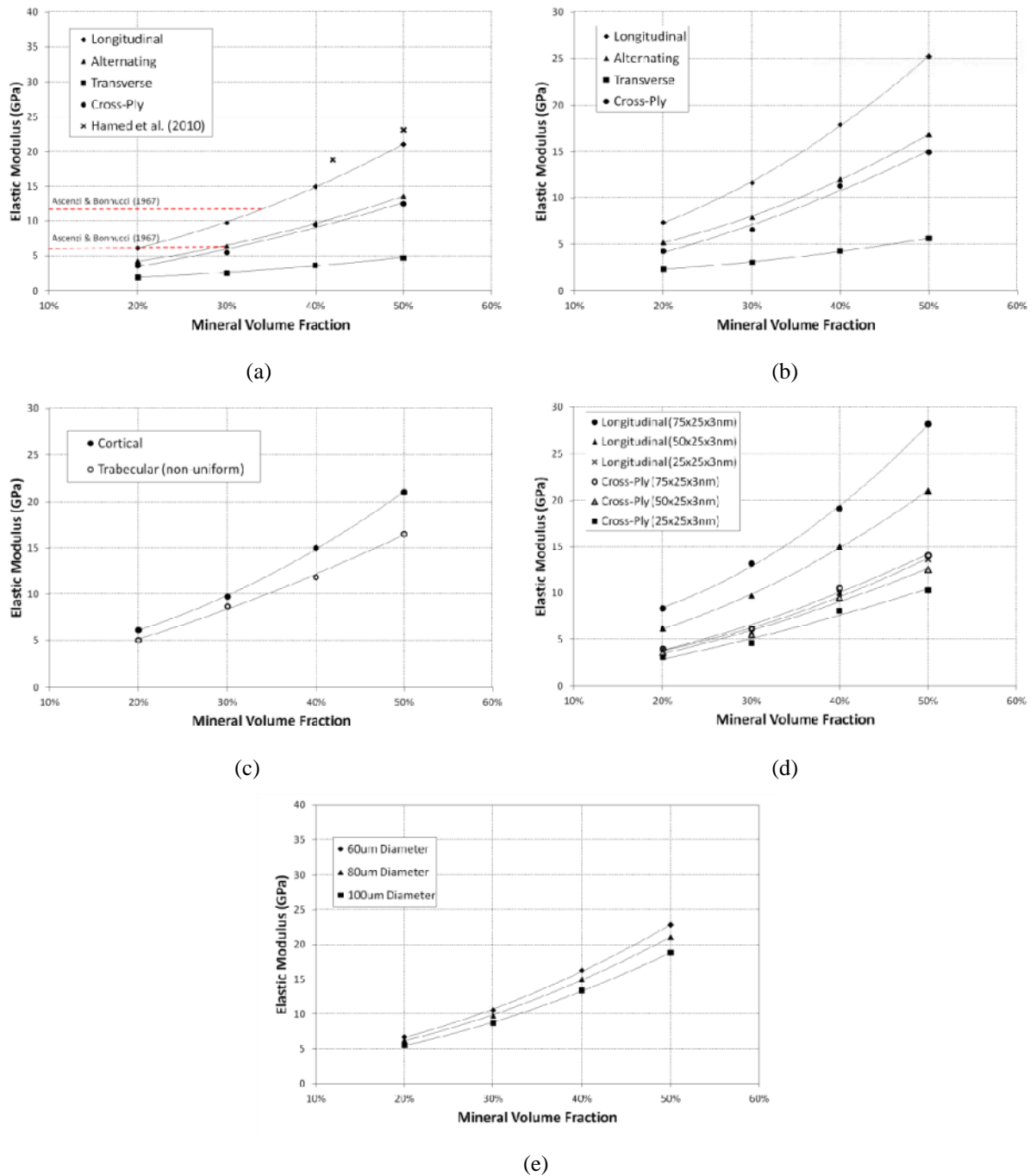


Figure 5: Results from two-step homogenisation which predicts the properties of bone as a function of mineral volume fraction: (a) Longitudinal modulus of various osteon arrangements and (b) longitudinal modulus of various trabecular arrangements (c) longitudinal modulus of cortical and trabecular tissue (non-uniform mineral distribution) with a longitudinal lamellar arrangement (d) effect of mineral aspect ratio on stiffness of longitudinal and cross-ply osteons and (e) effect of the Haversian canal diameter on the stiffness of longitudinal osteons (a second-order polynomial trendline has been fit to each set of data points).

Tables

Table 1: Constituent Material Properties

<i>Materials</i>	<i>Elastic Constants</i>	
Hydroxyapatite Crystals (Katz 1971)	$E_h = 114 \text{ GPa}$	$\nu_h = 0.28$
Collagen Matrix (Katz 1971)	$E_c = 1.2 \text{ GPa}$	$\nu_c = 0.35$

Table 2: Effective properties following one-step homogenisation at 40 % MVF

E_{11}	E_{22}	E_{33}	G_{12}	G_{23}	G_{13}
18.71 GPa	3.2 GPa	9.696 GPa	0.824 GPa	0.824 GPa	4.05 GPa
ν_{12}	ν_{23}	ν_{31}	ν_{21}	ν_{32}	ν_{13}
0.352	0.13	0.0823	0.0604	0.3965	0.1605

Table 3: Lamellar Orientations

<i>Arrangement</i>	<i>Relative Orientations</i>
Cross-Ply	[+45°/-45°/+45°/-45°/+45°/-45°/+45°/-45°]
Longitudinal	[+15°/-15°/+15°/-15°/+15°/-15°/+15°/-15°]
Transverse	[+75°/-75°/+75°/-75°/+75°/-75°/+75°/-75°]
Alternating	[+15°/-75°/+75°/-15°/+15°/-75°/+75°/-15°]